

# Diffusioosmosis of electrolyte solutions in uniformly charged channels

Evgeny S. Asmolov,<sup>1</sup> Elena F. Silkina,<sup>1</sup> and Olga I. Vinogradova<sup>1,\*</sup>

<sup>1</sup>*Frumkin Institute of Physical Chemistry and Electrochemistry,  
Russian Academy of Sciences, 31-4 Leninsky Prospekt, 119071 Moscow, Russia*

When the concentration of electrolyte solution varies along the channel the forces arise that drag the fluid toward the higher or lower concentration region inducing a flow termed diffusio-osmotic. This article investigates a flow that emerges in channels with constant density of surface charge  $\sigma$  and thin compared to their thickness electrostatic diffuse layers. An equation for the fluid flow rate  $Q$  is derived and used to describe analytically the flux of ions, and local potentials and concentrations. This equation, which allows to treat the diffusio-osmotic problems without tedious and time consuming computations, clarifies that the global flow rate is controlled only by the surface charge and concentration drop between the channel ends, and indicates that there always exist two different values of  $\sigma$  that correspond to a particular  $Q$ . Our theory provides a simple explanation of the directions of the fluid flow rate and ionic flux depending on the surface charge and diffusivity of ions, predicts a non-linear concentration distribution along the channel caused by convection, and relates it to the local potential changes by a compact formula. We also present and interpret the variations of the diffusio-osmotic velocity profiles and the apparent slip velocity along the channel and show that the latter is highly non-uniform and could even becomes alternating. The relevance of our results for diffusio-osmotic experiments and for some electrochemistry and membrane science issues is discussed briefly.

## I. INTRODUCTION

During recent decades, the pursuit of scale reduction has been extended to the fluidic domain and led to a rapid development of microfluidics and later nanofluidics [1–4]. These have posed an issue of finding the more efficient mechanisms of generating flows in thin channels that exhibit huge hydrodynamic resistance to a pressure-driven flow. One avenue for driving flow on such small scales is to exploit hydrodynamic slip [5–7]. Another promising avenue is to employ the so-called interfacially driven transport phenomena that emerge in response to gradients of an electric potential, concentration of a solute, etc [8]. The best known example is an electroosmosis, i.e. fluid flow induced by an applied (tangential) electric field. Diffusioosmosis is an alternative, and less explored, interfacially driven phenomenon that refers to flows under the gradient of a solute, for example a salt. An obvious advantage of diffusioosmosis is that it makes possible to convert chemical (osmotic) energy into mechanical one, i.e. to a directed flow of solvent, and does not require an external energy supply. The only source of energy is a concentration gradient of a solute, which is of much interest for such applications as water purification technologies, energy generation, lab-on-a-chip devices, and more [9, 10].

Despite its importance for several branches of surface physics and chemistry, as well as for applications, diffusioosmosis caused by a salinity gradient has so far received much less attention than electroosmosis. The successful understanding of its origin, due to Deryagin *et al.* [11] and Prieve *et al.* [12], was an important achievement

of 20th century colloidal hydrodynamics. Anticipating the discussion to follow in later, these authors have been the first to realize that in the case of electrolyte solutions there exist two contributions that originate the steady-state diffusioosmosis. The first one, termed chemiosmotic, is associated with the osmotic pressure gradient in the electrostatic diffuse layers (EDLs) formed in the neighborhood of the charged walls that extend to distances of the order of Debye length  $\lambda_D$  of the bulk electrolyte solution. The second contribution is associated with the electroosmosis under a spontaneously arising electric field that ensures the same propulsion velocity of ionic species of different diffusivity (which is equivalent to saying that the electric current vanishes). While the chemiosmotic flow is always toward the lower electrolyte concentration, the electroosmosis could be directed to any side depending on the difference in diffusivity of anions and cations, as well as on the sign of the surface charge.

During the past decades this scenario of diffusioosmosis has become widely accepted for electrolyte solutions. Nevertheless, the procedure of calculating the velocity of diffusio-osmotic flow is still beset with difficulties, especially in the case of channels of a finite thickness. To what extent can notions of a flow near a single wall be employed in confined systems? For example, should the condition of zero current be applied outside of the EDLs or differently? How do the concentration and emerging electric field vary along the channel? What is the velocity profile of a confined fluid and how does this depend upon the nature of the confining walls and concentration drop? There is a growing literature describing attempts to answer these questions and to provide a satisfactory quantitative theory of diffusioosmosis in a slightly nonuniform salt solution. We mention below what we believe are the more relevant contribution.

---

\* Corresponding author: oivinograd@yahoo.com

A large fraction of theoretical papers deal with an idealized case of a single, infinitely long, wall. Deryagin *et al.* [11] appear to have been the first to address the issue of diffusioosmotic flow caused by a gradient in the concentration of a simple salt and to argue that a spontaneous electric field emerges (to cancel the electric current far from the walls, i.e. beyond the EDLs, out), which, in turn, gives rise to a supplementary (electroosmotic) contribution to the total flow. These authors derived an equation that relates this emerging field with the ion diffusion coefficients, the local concentration of salt and its gradient in the bulk, but do not present any detailed results for a diffusio-osmotic velocity. A more systematic treatment of diffusioosmosis was contained in remarkable papers published by Prieve *et al.* [12] and Anderson [8]. The calculations [based on a system of the Nernst-Planck equations for the concentration of ion species, Poisson equation for the electric potential generated by inhomogeneous charge distribution and Stokes equation for fluid flow] led to an analytical solution for the local velocity of diffusio-osmotic plug flow far from the wall, i.e. outside of the diffuse layer. This outer velocity  $U_s$  was termed the diffusioosmotic slip velocity since macroscopically it appears that the liquid slips over the surface. The authors [12] have shown that the local parameters determining both contributions to this (apparent) slip velocity are the surface potential, bulk concentration of salt and its gradient, but have not tried to derive them self-consistently. This was taken up later by Keh and Ma [13] who obtained a solution for  $U_s$  by postulating a linear variation in bulk concentration along the wall. However, no attempts have been made to explain how to impose such a constant gradient externally and/or whether could it naturally occur.

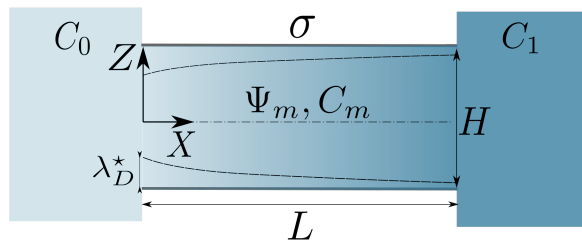


FIG. 1. Sketch of the microchannel of thickness  $H$ , length  $L \gg H$  and constant surface charge density  $\sigma$  that connects the “fresh” (left) and “salty” (right) bulk electrolyte reservoirs of concentrations  $C_0$  and  $C_1$ . The extension of electrostatic diffuse layers, which is of the order of the Debye length  $\lambda_D \ll H$  and takes its upper value  $\lambda_D = \lambda_D^*$  at  $X = 0$  by reducing along the channel. The electroneutral central area is of “bulk” concentration  $C_m$  and potential  $\Psi_m$ , both depend on  $X$ .

During the last years several theoretical papers have been concerned with the diffusio-osmotic flow in a planar channel of finite thickness  $H$  and length  $L$  connecting two reservoirs of different salinity (as sketched in Fig. 1). Ma and Keh [14] and Keh [15] address themselves to the problem of the diffusio-osmotic flow in a thick ( $H \gg \lambda_D$ )

channel. These authors performed detailed calculations of  $U_s$  assuming that the electric current has to vanish locally, i.e. at any point of the channel. Later, however, Jing and Das [16] argued that in the case of channel of finite thickness it would be more appropriate to apply the zero net (i.e. averaged over a cross-section) current condition. Note that neither paper attempted to relax the simplifying assumption about a constant concentration gradient along the channel or address itself to the issue of its calculation. While this conventional assumption appears to be reasonable for a small difference between bulk concentrations of reservoirs, it is by no means obvious in the most interesting and practically relevant case of a finite concentration drop. In any event, it seems clear that the variation in the concentration gradient along the channel and local concentrations are established self-consistently and have to be calculated. Ault *et al.* [17] performed the calculations for a constant surface potential channel and found that the local concentration inside varies non-linearly. These authors, however, made an assumption that the fluid flow rate is initially prescribed and have not attempted to derive it. We are unaware of any theoretical work that addressed this issue.

Numerical calculations might be expected to shed some light on diffusio-osmotic phenomena, and indeed in prior investigations numerical approaches have mostly been followed. The diffusio-osmotic velocity has been computed from a solution to a system of partial differential equations establishing linear relationships between local fluxes averaged across channel cross-sections (the current, the fluxes of fluid and ions) and driving forces (electric field, gradients of salt concentration and pressure) [16, 18–20]. The significance of Prieve *et al.* [12] paper does not seem to be recognized in these publications. Most subsequent attempts at improvements on numerical calculations of the diffusio-osmotic flow [21–23] have also either ignored or failed to make direct connection with earlier analytical results [8, 12, 14].

Given the current upsurge of the interest in the diffusio-osmotic phenomena and their applications it would seem appropriate to bring more theoretical analysis to bear on this problem. In this paper we present some results of a study of the steady-state diffusio-osmotic flow in the channel of a constant surface charge density assuming thin diffuse layers compared to its thickness, but do not make any simplifying assumptions about the magnitudes of the surface potential and the concentration drop between the reservoirs. Our theory is based on an approach introduced originally by Prieve *et al.* [12] in their study of a local diffusio-osmotic slip near a single wall. We shall see that the extension of the theory to the two-wall case provides new insight into the physics of diffusioosmosis yielding useful (approximate) analytical results, as well as suited to numerical work. These features are especially advantageous when one is attempting to calculate the diffusio-osmotic velocity at a large concentration drop.

Our paper is arranged as follows: In Sec. II we de-

fine our system and formulate the governing equations. Section III discusses the perturbation of the electrostatic potential due to diffuse layers. Derivations of equations for the local surface potentials are given. In Sec. IV the extension of the Prieve *et al.* [12] approach to two walls is described and the equation for the local diffusio-osmotic mobility profile is derived. The differential equation for the local diffusio-osmotic slip is also formulated here. Section V describes the theory of a global diffusio-osmotic flow in the channel. In Sec. V A some general considerations concerning the flow rate of fluids and ionic flux in the channel are given. Here we also argue that the zero current condition should be imposed to its average (over the cross-section) value. The procedure for calculating the concentration and potential in the electroneutral (“bulk”) part of the channel is described in Sec. V B. After establishing a relationship between the distributions of potential and concentration in the “bulk” part of the channel, we obtain an expression that relates the latter to the flow rate of fluid, which can be easily found by integrating a simple function we derive. Since the calculated concentration distributions along the channel are, in general, nonlinear, to provide the same flow rate in every cross-section the pressure gradient arises naturally in our analysis by giving rise to a supplementary flow. In Sec. V C the form of the velocity profiles is described; this depends on the locus of the given cross-section since the pressure gradient is alternating. We also consider the apparent slip velocity on the walls and discuss its variations along the channel in different situations. Finally, we propose simple and compact analytical approximations for the diffusio-osmotic slip velocity, which apply when the surface potential becomes small. We conclude in Sec. VI with a discussion of our results and their relevance.

## II. MODEL AND GOVERNING EQUATIONS

We consider a system sketched in Fig. 1. A planar channel of thickness  $H$  and length  $L \gg H$  is in contact with low (left) and high (right) salinity reservoirs of symmetric 1:1 salt solutions of concentrations (number densities of salt molecules)  $C_0$  and  $C_1$  at standard temperature  $T$ . Both solutions are of the same dynamic viscosity  $\eta$  and permittivity  $\varepsilon$ .

It is convenient to place the origin of coordinates in the midplane of the channel at a junction with the low-salinity bath. The  $Z$ -axis is aligned across the slit, so the two walls are located at  $Z = \pm H/2$ , and for a symmetric channel it is enough to consider  $0 \leq Z \leq H/2$ . The  $X$ -axis is defined along the channel, and  $0 \leq X \leq L$ .

For a given thickness  $H$  and length  $L$  the solution inside the slit will adopt the configuration (i.e. distributions of the number density of the ionic species  $C^\pm$ , electrostatic potential  $\Psi$  and hydrostatic pressure  $P$ ) that minimizes the energy dissipation, i.e. corresponds to steady-state diffusioosmotic flow with the velocity  $\mathbf{U}$ .

The scenario of a stationary diffusio-osmosis can be

understood as follows. When we connect low and high salinity reservoirs, cations and anions begin to diffuse along the channel towards the “fresh” bath, but their diffusion coefficients  $D^+$  and  $D^-$  are generally unequal. Ions with larger diffusion coefficients migrate faster, but a local ionic concentration can approach the steady-state if and only if their fluxes at any cross-section are equal. This is equivalent to saying that no electric current occurs throughout the channel. To provide this, a tangential electric field should emerge to accelerate slower ions and retard faster ones. This field gives rise to an electroosmotic flow along the channel. Simultaneously, the osmotic pressure gradient occurring within the EDLs and balanced by the viscous stress induces a chemiosmotic flow from the “salty” to “fresh” reservoir. In addition, a hydrostatic pressure distribution along the channel emerges. These contributions are superimposed, and the stationary state of resulting diffusio-osmotic flow is described by the system of several governing equations specified below.

The Nernst-Planck (or convection-diffusion) equation describes the conservation of ionic species at each point  $(X, Z)$  inside the channel

$$\nabla \cdot \mathbf{J}^\pm = 0, \quad (1)$$

where the ionic fluxes  $\mathbf{J}^\pm$  of cations and anions are given by

$$\mathbf{J}^\pm = C^\pm \mathbf{U} + D^\pm \left( -\nabla C^\pm \mp \frac{e}{k_B T} C^\pm \nabla \Psi \right). \quad (2)$$

Here  $e$  is the elementary positive charge and  $k_B$  is the Boltzmann constant. The first term in Eq. (2) is associated with the convective flux of ions induced by the flow, the second refers to the diffusive drift relative to a solvent, and the third one is due to migration of ions in the emerging electric field.

The relation between the potential  $\Psi$  and the charge density  $\rho$  is given by the Poisson equation:

$$\Delta \Psi = -\frac{\rho}{4\pi\varepsilon} = -\frac{e(C^+ - C^-)}{4\pi\varepsilon}. \quad (3)$$

The fluid flow satisfies the Stokes equations,

$$\nabla \cdot \mathbf{U} = 0, \quad (4)$$

$$\eta \Delta \mathbf{U} - \nabla P = \rho \nabla \Psi. \quad (5)$$

It is clear that the theory for the diffusio-osmosis requires, as input, the hydrodynamic and electrostatic boundary conditions at the channel walls. Here we consider no-slip ( $\mathbf{U} = \mathbf{0}$  at  $Z = \pm H/2$ ) nonconducting surfaces of charge density  $\sigma$ , which is constant, i.e. independent on  $X$ . Rather than using  $\sigma$  explicitly we here describe the surfaces by the Gouy-Chapman length

$$\ell_{GC} = \frac{e}{2\pi\sigma\ell_B}, \quad (6)$$

where  $\ell_B = \frac{e^2}{\epsilon k_B T}$  is the Bjerrum length. The Gouy-Chapman length is inversely proportional to the surface charge density (and may be positive or negative depending on its sign).

The partial differential equations (1)-(5) we have described above are generic and apply at any point  $(X, Z)$  of the channel of an arbitrary thickness. They can generally be solved only numerically. However, below we show that approximate analytical results can be obtained in the limit of thick channel, which, essentially, implies that a compensating charge of the opposite sign and equal magnitude staying in the neighborhood of the charged walls is confined in very thin electrostatic diffuse layers (EDLs) near the walls, while an extended central region of the channel is then, to the leading order, electro-neutral (“bulk”) in any cross-section. This implies that at any  $X$  it is admissible to divide the thick channel into a surface (inner) and a bulk (or outer) regions. The concentration  $C_m$  and potential  $\Psi_m$  in the bulk region are then independent on  $Z$  and vary slowly in the  $X$ -direction.

The local EDL thickness is of the order of the Debye screening length at a given cross-section and can be defined as

$$\lambda_D = [8\pi\ell_B C_m]^{-1/2} \propto C_m^{-1/2}, \quad (7)$$

Clearly,  $\lambda_D$  reduces on increasing  $X$  since the concentration augments. The upper value of  $\lambda_D$  is thus attained at  $X = 0$ . In this cross-section  $C_m = C_0$  that yields

$$\lambda_D^* = [8\pi\ell_B C_0]^{-1/2}. \quad (8)$$

Therefore, to fulfil the thick channel condition, it is enough to require  $\lambda_D^* \ll H$ .

Note that by analyzing the experimental data it is more convenient to use the concentration  $\mathcal{C}$  [mol/l], which is related to  $C$  as  $C \simeq N_A \times 10^3 \times \mathcal{C}$ , where  $N_A$  is Avogadro’s number. The Bjerrum length of water at  $T \simeq 298$  K is equal to about 0.7 nm leading to

$$\lambda_D^* [\text{nm}] \simeq \frac{0.305 [\text{nm}]}{\sqrt{\mathcal{C}_0 [\text{mol/l}]}}, \quad (9)$$

Upon increasing  $\mathcal{C}_0$  from  $10^{-6}$  to 1 mol/l the screening length reduces from about 300 down to 0.3 nm. This implies that if, say, we take  $H = 100$  nm, then the thick channel limit is expected when  $\lambda_D^* \leq 10$  nm, i.e. provided that in the “fresh” bath  $\mathcal{C}_0 \geq 10^{-3}$  mol/l. In all calculations below we fix this value of  $H$  and use  $\mathcal{C}_0 = 10^{-3}$  mol/l.

In the thick channel limit the local electrostatic potential in the slit is given by

$$\Psi(X, Z) = \Psi_m(X) + \Phi(X, Z). \quad (10)$$

Here the “bulk” term ( $\Psi_m$ ) is supplemented by a “surface” term ( $\Phi$ ) that represents the perturbation due to

diffuse layers. Eq. (10) implies that the emerging electric field that produce electroosmotic flow is additively superimposed upon the field of the EDL. Later we shall see that for our configuration  $\Phi$  is independent on the fluid flow.

To construct the solution of the system of Eqs. (1)-(5) it is convenient to define the dimensionless coordinates

$$x = \frac{X}{L}, \quad z = \frac{2Z}{H}$$

that vary from 0 to 1. The dimensionless potentials are defined as

$$\psi = \frac{e\Psi}{k_B T}, \quad \phi = \frac{e\Phi}{k_B T}.$$

We also introduce the dimensionless variables [24]

$$\mathbf{j}^\pm = \mathbf{J}^\pm \frac{2L}{C_0(D^+ + D^-)}, \quad c^\pm = \frac{C^\pm}{C_0},$$

$$\mathbf{u} = \mathbf{U} \frac{4\pi\eta e^2 L}{\epsilon k_B^2 T^2}, \quad p = P \frac{\pi e^2 H^2}{\epsilon k_B^2 T^2}$$

### III. ELECTROSTATIC POTENTIAL

Using the dimensionless variables the Nernst-Planck (1) and the continuity (4) equations can be rewritten as

$$\frac{H}{2L} \partial_x j_x^\pm + \partial_z j_z^\pm = 0, \quad (11)$$

$$\frac{H}{2L} \partial_x u_x + \partial_z u_z = 0. \quad (12)$$

For a long channel,  $H/L \ll 1$ , the leading-order terms in Eqs. (11) and (12) involve only derivatives with respect to  $z$ .

Applying the impermeability condition

$$j_z^\pm(x, \pm 1) = u_z(x, \pm 1) = 0, \quad (13)$$

we conclude that the normal fluxes  $j_z^\pm$  and velocity  $u_z$  are of the order of  $H/L$ , i.e. small. Since  $j_z^\pm \simeq 0$ , the ion concentrations obey local Boltzmann distributions at any cross-section [18, 20]:

$$c^\pm = c_m(x) \exp(\mp \phi), \quad (14)$$

where

$$\phi = \psi(x, z) - \psi_m(x), \quad (15)$$

which is Eq. (10) rewritten in dimensionless form. Here the midplane (“bulk”) concentration  $c_m$  and the potential  $\psi_m$  vary only in  $x$  direction. The boundary conditions for  $c_m$  are

$$c_m(0) = 1, \quad c_m(1) = c_1 = C_1/C_0. \quad (16)$$

We also set

$$\psi_m(0) = 0, \quad (17)$$

but the value of  $\psi_m(1)$  that ensures the fulfillment of the condition of zero current is initially unknown and has to be determined.

The potential  $\phi$  satisfies the Poisson-Boltzmann equation at each cross-section,

$$\partial_{zz}\psi = \partial_{zz}\phi = c_m(x) \lambda^{-2} \sinh \phi, \quad (18)$$

$$\lambda = \frac{2\lambda_D^*}{H}.$$

To integrate Eq. (18) we impose two electrostatic boundary conditions. Symmetry of the channel dictates that

$$\partial_z\psi(x, 0) = \partial_z\phi(x, 0) = 0.$$

Another condition requires a constant surface charge density of the walls, which is equivalent to a constant gradient of the surface potential.

$$\partial_z\psi(x, 1) = \partial_z\phi(x, 1) = \frac{H}{\ell_{GC}}. \quad (19)$$

However, the surface potential itself varies with  $x$  since a local Debye length scales with  $c_m^{-1/2}$ .

The first integration of the Poisson-Boltzmann equation (18) from 0 to  $z$  leads to

$$\frac{(\partial_z\phi)^2}{2} = c_m \lambda^{-2} (\cosh \phi - 1) = 2c_m \lambda^{-2} \sinh^2\left(\frac{\phi}{2}\right) \quad (20)$$

or

$$\partial_z\phi = 2\lambda^{-1} c_m^{1/2} \sinh\left(\frac{\phi}{2}\right) \quad (21)$$

This equation is identical to that for a single wall, although the boundary conditions were different [in the single wall problem both  $\phi$  and  $\partial_z\phi$  vanish far away from the wall].

From Eqs. (19) and (21) it follows that the relation between the surface potential and charge is given by

$$\phi_s = 2 \operatorname{arsinh}\left(\frac{\lambda_D^*}{c_m^{1/2} \ell_{GC}}\right), \quad (22)$$

which can be regarded as a direct analog of the Grahame equation for a single wall [25].

Note that  $\lambda_D^*/(c_m^{1/2} \ell_{GC})$  plays a role of an effective surface charge density that reduces on increasing  $x$ . When it is small, Eq. (22) can be written as

$$\phi_s(x) \simeq \frac{2\lambda_D^*}{c_m^{1/2} \ell_{GC}} = \frac{\lambda H}{c_m^{1/2} \ell_{GC}} \ll 1. \quad (23)$$

If the effective surface charge is large, the surface potential depends on it weakly logarithmically:

$$\phi_s(x) \simeq \pm 2 \ln \left[ \frac{2\lambda_D^*}{c_m^{1/2} |\ell_{GC}|} \right] = \pm 2 \ln \left[ \frac{\lambda H}{c_m^{1/2} |\ell_{GC}|} \right] \quad (24)$$

The choice of sign in (24) depends on whether the walls are positively or negatively charged. The plus sign must be taken for a positive  $\ell_{GC}$ , and vice versa.

Performing the integration in (21) yields an exact analytical solution for the disturbance potential

$$\phi(x, z) = 4 \operatorname{artanh} \left[ e^{(z-1)c_m^{1/2}/\lambda} \tanh\left(\frac{\phi_s}{4}\right) \right], \quad (25)$$

where  $\phi_s$  is given by (22).

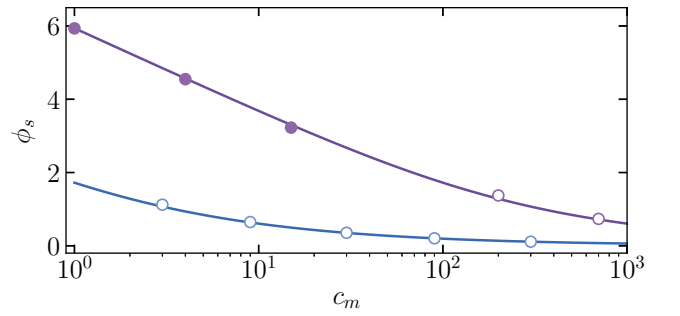


FIG. 2. Surface potential  $\phi_s$  as a function of  $c_m$  computed using  $\ell_{GC} = 1$  and  $10$  nm (solid curves from top to bottom) for  $C_0 = 10^{-3}$  mol/l and  $C_1 = 1$  mol/l. Open and filled circles show calculations from Eqs. (23) and (24).

A plot of  $\phi_s(c_m)$  is given in Fig. 2. For this numerical example we use  $H = 100$  nm and perform calculations from Eq. (18) for channels of  $\ell_{GC} = 1$  and  $10$  nm that connect reservoirs of concentrations  $C_0 = 10^{-3}$  mol/l and  $C_1 = 1$  mol/l. The calculations from (22) are also made, but not shown since they fully coincide with numerical results. It can be seen that on increasing  $c_m$  (and hence  $x$ ) the surface potential reduces and that at a given “bulk” concentration it is always higher for surfaces of smaller  $\ell_{GC}$ . Also included in Fig. 2 are approximate surface potentials predicted by Eqs. (23) and (24). The fits are quite good for small and large  $\phi_s$ , correspondingly, which is expected since  $\lambda_D^* \simeq 10$  nm is much smaller than  $H$ .

#### IV. LOCAL DIFFUSIO-OSMOTIC SLIP

From (18) it follows that  $x$ -momentum equation (5) can be transformed into a linear differential equation [12, 16]

$$\partial_{zz}u_x = \partial_x p - \frac{c_m \sinh \phi}{\lambda^2} \partial_x \psi_m + \frac{\cosh \phi - 1}{\lambda^2} \partial_x c_m. \quad (26)$$

Here the hydrodynamic (pressure-driven) term is supplemented by an electroosmotic one and a chemiosmotic contribution.

Integrating this equation twice with respect to  $z$  and applying the no-slip  $u_x(1) = 0$  and symmetry  $\partial_z u_x(0) = 0$  boundary conditions we derive

$$u_x = m_h \partial_x p + m_e \partial_x \psi_m + m_c \partial_x c_m, \quad (27)$$

where the local hydrodynamic and electroosmotic mobilities are given by

$$m_h = -\frac{1-z^2}{2}, \quad (28)$$

$$m_e = -\phi + \phi_s. \quad (29)$$

The latter equation implies that the sign of  $m_e$  is defined solely by that of  $\phi_s$ . An electroosmotic mobility will be positive for positively charged surfaces and negative for negatively charged.

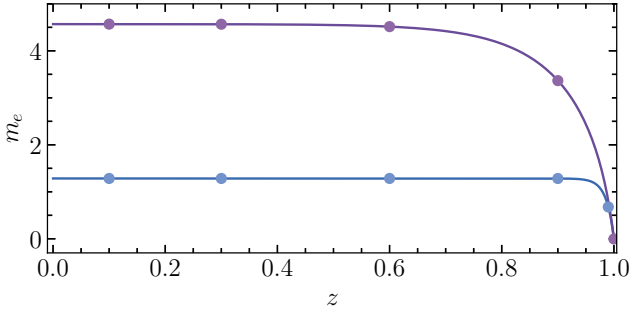


FIG. 3. Electroosmotic mobility profiles computed for cross-sections of  $C_m = 4 \times 10^{-3}$  and 0.2 mol/l (solid curves from top to bottom) for the upper curve in Fig. 2. Circles show  $m_e$  calculated from Eq. (29) using (22) and (25).

Figure 3 shows the electroosmotic mobility profiles computed with the same parameters as for the upper curve in Fig. 2. The calculations are made for cross-sections of  $C_m = 4 \times 10^{-3}$  and 0.2 mol/l, which corresponds to  $c_m = 4$  and 200. The numerical curves are perfectly described by Eq. (29) with  $\phi_s$  and  $\phi$  calculated from (22) and (25). It can be seen that the (positive) electroosmotic mobility in the central region shows a distinct plateau and varies only inside the EDLs to vanish at the walls. On reducing  $C_m$  the plateau height decreases, which reflects the variation in  $\phi_s$ , but remains finite for both specimen examples presented in Fig.3.

The local chemiosmotic mobility may, in turn, be determined from

$$m_c = -\frac{1}{\lambda^2} \int_z^1 \int_0^y [\cosh \phi(s) - 1] ds dy \quad (30)$$

using Eq. (20). Performing the first integration yields

$$\begin{aligned} \int_0^y (\cosh \phi - 1) ds &= \lambda c_m^{-1/2} \int_0^y \sinh(\phi/2) d\phi \\ &= 2\lambda c_m^{-1/2} [\cosh(\phi/2) - 1]. \end{aligned}$$

The second integral can then be calculated as follows

$$\begin{aligned} m_c &= -c_m^{-1} \int_\phi^{\phi_s} \frac{\cosh(\phi/2) - 1}{\sinh(\phi/2)} d\phi \\ &= -4c_m^{-1} \{ \ln [\cosh(\phi_s/4)] - \ln [\cosh(\phi/4)] \}. \end{aligned} \quad (31)$$

Since the expression in curly brackets is positive for any  $\phi_s \neq 0$ , we conclude that the chemiosmotic mobility can only be negative.

In the case of low surface potentials,  $|\phi_s| \leq 1$ , one can use the approximation  $\ln [\cosh(\phi/4)] \simeq \phi^2/32$ . Equation (32) then reduces to

$$m_c \simeq -\frac{\phi_s^2 - \phi^2}{8c_m} \ll 1 \quad (33)$$

Thus, the chemiosmotic mobility turns out to be small compared to the electroosmotic one [given by Eq. (29)].

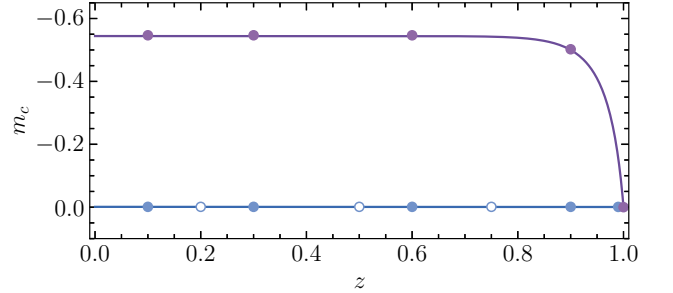


FIG. 4. Chemiosmotic mobility  $m_c$  as a function of  $z$  computed with the same parameters as in Fig. 3. Filled and open circles are calculations from Eqs. (32) and (33).

Figure 4 includes numerical curves for a local chemiosmotic mobility calculated with the same parameters as in Fig. 3. The shape of these curves for (negative)  $m_c$  is similar to that for electroosmotic mobility, so that we do not discuss it in detail, but note that for both cross-sections  $|m_c|$  is smaller than unity (and significantly below  $m_e$ ). Both curves now are well fitted by Eq. (32). Also included in Fig. 4 is the chemiosmotic mobility calculated from asymptotic Eq. (33). The fit is good for the lower curve ( $C_m = 0.2$  mol/l), but clearly, the exact results for the upper curve ( $C_m = 4 \times 10^{-3}$  mol/l) should be irreconcilable with Eq. (33) since  $\phi_s \simeq 4.5$  is finite. Indeed, there is some discernible discrepancy in the direction of greater  $|m_c|$  (not shown).

The above equations for mobilities apply at any point of the channel, but since  $\phi$  vanishes outside the EDLs,

we might argue that in the central electroneutral region Eqs. (29) and (32) reduce to

$$m_e \simeq \phi_s, \quad m_c \simeq -\frac{4 \ln [\cosh (\phi_s/4)]}{c_m}. \quad (34)$$

The sum of electro- and chemiosmotic mobilities, Eqs. (29) and (32), corresponds to diffusio-osmotic plug flow with dimensionless slip velocity,

$$u_s = \phi_s \partial_x \psi_m - 4 \frac{\partial_x c_m}{c_m} \ln \left[ \cosh \left( \frac{\phi_s}{4} \right) \right], \quad (35)$$

where given by (22) surface potential  $\phi_s$  is salt-dependent. It becomes evident that, if  $\phi_s = 0$ , both terms vanishes, so the diffusioosmotic flow does not emerge. We remark that it also cannot be generated if electro- and chemiosmotic contribution cancel each other. It is of considerable interest to determine whether and when this could happen. In all other situations  $u_s \neq 0$ , and at this stage it is not clear will it be positive or negative for some special configuration. While the chemiosmotic contribution can only be negative (since the derivative  $\partial_x c_m$  is positive), the electro-osmotic term can be of any sign depending on  $\partial_x \psi_m$ , which is still unknown. One further comment should be made. Eq. (35) is non-linear in  $c_m$ . This implies that in the general case the diffusio-osmotic slip velocity varies along the channel.

We recall that the above treatment corresponds to cross-sections of fixed  $c_m$ . However, they are defined by coordinate  $x$ , and hence we have to relate the (“bulk”) potential  $\psi_m$ , concentration  $c_m$  and their derivatives to  $x$ , which requires further investigation. These functions of  $x$  can only be found from the solution of the global problem for the whole channel by imposing boundary conditions (16) and (17), as well as the zero total current condition. Once they are determined,  $\phi_s(x)$  can be obtained by using Eq. (22), and hence  $u_s(x)$  from Eq. (35).

## V. GLOBAL DIFFUSIO-OSMOTIC FLOW

### A. General considerations

We focus first to the expressed per unit channel thickness ion fluxes  $\mathcal{J}^\pm$  and flow rate  $\mathcal{Q}$  of the fluid, which can be written as

$$\mathcal{J}^\pm = \frac{1}{2} \int_{-1}^1 j_x^\pm dz, \quad \mathcal{Q} = \frac{1}{2} \int_{-1}^1 u_x dz, \quad (36)$$

Integrating Eqs. (11) and (12) and making use of (36) we find

$$\frac{H}{2L} \partial_x \mathcal{J}^\pm + \int_{-1}^1 \partial_z j_z^\pm dz = 0, \quad (37)$$

$$\frac{H}{2L} \partial_x \mathcal{Q} + \int_{-1}^1 \partial_z u_z dz = 0. \quad (38)$$

From impermeability condition (13) it follows that the integrals in Eqs. (37) and (38) are zero:

$$\int_{-1}^1 \partial_z j_z^\pm dz = j_z^\pm(1) - j_z^\pm(-1) = 0,$$

$$\int_{-1}^1 \partial_z u_z dz = u_z(1) - u_z(-1) = 0.$$

Thus,

$$\partial_x \mathcal{J}^\pm = 0, \quad (39)$$

$$\partial_x \mathcal{Q} = 0. \quad (40)$$

The last equations imply that  $\mathcal{J}^\pm$  and  $\mathcal{Q}$  given by (36) do not vary with  $x$ , i.e. are the same at any cross-section. This integral representation of the Nernst-Planck and continuity equations can be used to determine the distributions of concentration  $c_m(x)$  and potential  $\psi_m(x)$  along the channel.

The value of  $\mathcal{J}^\pm$  may be determined by substituting  $j_x^\pm$  into (36) and performing the integration. These  $x$ -components of ion fluxes are given by (2) and can be rewritten in the dimensionless form as,

$$j_x^\pm = c^\pm \text{Pe} u_x + (1 \pm \beta) (-\partial_x c^\pm \mp c^\pm \partial_x \psi), \quad (41)$$

where

$$\text{Pe} = \frac{\varepsilon k_B^2 T^2}{2\pi\eta e^2 (D^+ + D^-)} \quad (42)$$

is the Péclet number that characterizes the ratio of the rate of convection by that of diffusion and the (ion specific) factor  $\beta$  is defined in terms of the difference in diffusion constants of cations and anions

$$\beta = \frac{D^+ - D^-}{D^+ + D^-}, \quad (43)$$

In such a definition  $\beta$  is positive, if cations diffuse faster than anions, and vice versa. The values of  $\beta$  are typically confined between  $-1$  to  $1$ . For instance,  $\beta \simeq 0.285$  for  $\text{KCH}_3\text{COO}$ ,  $0.014$  for  $\text{KNO}_3$ ,  $-0.207$  for  $\text{NaCl}$ , and nearly vanishes for  $\text{KCl}$  [26]. We also emphasize that for a specific salt  $\text{Pe}$  is controlled by  $D^+ + D^-$  and is a constant. Substituting the experimental values for diffusion coefficients [26] into Eq. (42) we obtain for the above inorganic salts  $\text{Pe} \simeq 0.31, 0.25, 0.28$ , and  $0.23$ , correspondingly. These values are quite close, and we also note that although  $\text{Pe} < 1$ , it is not too small to be neglected.

We remark and stress that Eqs. (39) and (41) imply that the zero current condition must refer to the average current  $\mathcal{J}^+ - \mathcal{J}^- = 0$ , as suggested by Jing and Das [16], but not to the local values  $j_x^+ - j_x^-$ , as proposed by Keh and Ma [13].

## B. “Bulk” concentration, potential and pressure

We now turn to the derivation of the equations for  $c_m$ ,  $\psi_m$  and  $p$  as a function of  $x$ , which are required to calculate the fluid velocity.

For a thick channel the main contributions to  $\mathcal{J}^\pm$  and  $\mathcal{Q}$  are coming from its central (“bulk”) part, where the fluid velocity is the sum of the plug diffusio-osmotic and parabolic pressure-driven velocities:

$$u_x \simeq u_s - \frac{1 - z^2}{2} \partial_x p.$$

Consequently, the flow rate that obeys Eq. (40) is given by

$$\mathcal{Q} \simeq u_s - \frac{\partial_x p}{3}. \quad (44)$$

As we have clarified in Sec. IV, in the general case the slip velocity varies along the channel. Consequently, the constant flow rate can only be provided if the local pressure gradient is non-zero. Moreover, one can argue that since the hydrostatic pressure in both reservoirs are equal, the function  $p(x)$  should take its extremum value at some  $x$ .

Integrating Eq. (41) over  $z$  and using that

$$\int_{-1}^1 c^\pm u_x dz \simeq c_m \mathcal{Q},$$

one obtains

$$\mathcal{J}^+ \simeq c_m \text{Pe} \mathcal{Q} + (1 + \beta) (-\partial_x c_m - c_m \partial_x \psi_m), \quad (45)$$

$$\mathcal{J}^- \simeq c_m \text{Pe} \mathcal{Q} + (1 - \beta) (-\partial_x c_m + c_m \partial_x \psi_m). \quad (46)$$

Introducing  $\mathcal{J} = \mathcal{J}^\pm$ , one can exclude  $\mathcal{Q}$  by subtracting these equations to get

$$\partial_x \psi_m = -\beta \frac{\partial_x c_m}{c_m}. \quad (47)$$

Substituting Eq. (47) into Eq. (35) we find that this expression for a diffusio-osmotic slip velocity can be reformulated as

$$u_s = -\frac{\partial_x c_m}{c_m} \left[ \beta \phi_s + 4 \ln \left[ \cosh \left( \frac{\phi_s}{4} \right) \right] \right]. \quad (48)$$

While the form of Eqs. (47) and (48) is identical to the known formulas for a single wall [8, 12], the boundary conditions and the derivation itself are different.

Further insight can be gained by integrating Eq. (47) and imposing condition (16), which yields

$$\psi_m = -\beta \ln c_m. \quad (49)$$

Using this equation we can immediately obtain the mid-plane potential at the “salty” end, which is equal to the voltage  $\Delta\psi_m = \psi_m(1) - \psi_m(0)$  between reservoirs. The

later is given by  $\Delta\psi_m = -\beta \ln c_1$ . To get some idea of the orders of magnitude, with the parameters of Fig. 2 we obtain  $\Delta\psi_m \simeq 1.4$  for NaCl and  $-0.1$  for KNO<sub>3</sub>. Clearly, the quantity  $\Delta\psi_m$  should be practically zero for KCl since  $\beta \simeq 0$ . The form of the above expression for  $\Delta\psi_m$  is analogous to the known electrochemistry formula for the diffusion potential between two salt solutions (separated by an infinitesimally thin uncharged membrane) derived for the situation of zero  $\mathcal{Q}$ . Here we have shown that the same expression applies when  $\mathcal{Q} \neq 0$  too. Returning to generic Eq. (49), we emphasize that it describes  $\psi_m$  at any cross-section inside the channel, but not just its ends (and is valid at any flow rate of fluid). As a side note, Eq. (49) is similar to the expression describing the potential distribution around catalytic particles that release ions [27, 28]. However, we are unaware of any prior work that has derived it for a diffusio-osmotic flow in a thick slit.

Substituting (49) into (45) we obtain an ordinary differential equation

$$\mathcal{J} = c_m \text{Pe} \mathcal{Q} - (1 - \beta^2) \partial_x c_m \quad (50)$$

that provides a route to the determination of  $c_m(x)$ .

In the special case of  $\mathcal{Q} = 0$  the solution to Eq. (50) satisfying boundary conditions (16) yields

$$\mathcal{J} = -(1 - \beta^2) (c_1 - 1) \quad (51)$$

and

$$c_m = 1 - \frac{\mathcal{J}}{1 - \beta^2} x = 1 + (c_1 - 1) x. \quad (52)$$

We emphasize that when  $\mathcal{Q}$  vanishes,  $\mathcal{J}$  is negative, i.e. toward the “fresh” bath, and the (bulk) concentration  $c_m$  augments linearly with  $x$ .

The emergence of diffusio-osmotic flow, however, normally implies that  $\mathcal{Q} \neq 0$ . By integrating Eq. (50) and applying the first boundary condition in (16) we derive

$$c_m = \left( 1 - \frac{\mathcal{J}}{\text{Pe} \mathcal{Q}} \right) \exp \left( \frac{\text{Pe} \mathcal{Q}}{1 - \beta^2} x \right) + \frac{\mathcal{J}}{\text{Pe} \mathcal{Q}}. \quad (53)$$

The flux  $\mathcal{J}$  can then be found from (53) by using the second boundary condition in (16)

$$\mathcal{J} = \text{Pe} \mathcal{Q} \frac{c_1 - c^*}{1 - c^*}, \quad (54)$$

where the quantity

$$c^* = \exp \left( \frac{\text{Pe} \mathcal{Q}}{1 - \beta^2} \right) \quad (55)$$

defines the sign of  $\mathcal{J}$ , i.e. the direction of ionic flux. Thus  $c^* < 1$  for  $\mathcal{Q} < 0$  that yields a negative  $\mathcal{J}$ . However,  $c^* > 1$  for  $\mathcal{Q} > 0$ , so the sign of  $\mathcal{J}$  is the same as that of  $c_1 - c^*$ . Note that Eq. (51) can be reproduced by expanding (54) about  $\mathcal{Q} = 0$  and taking the leading order term only. Recall that zero  $\mathcal{Q}$  yields  $\mathcal{J} < 0$ .



We also remark that from Eq. (53) it follows that, if  $x \ll 1$ , even for a finite flow rate the concentration becomes linear in  $x$

$$c_m \simeq 1 - \frac{(c_1 - 1)\text{Pe}\mathcal{Q}}{(1 - c^*)(1 - \beta^2)}x. \quad (56)$$

The same is true close to the “salty” end, where  $x$  is close to unity

$$c_m \simeq c_1 - \frac{(c_1 - 1)c^*\text{Pe}\mathcal{Q}}{(1 - c^*)(1 - \beta^2)}(x - 1), \quad (57)$$

but not for the whole channel.

Equation (53) can be regarded as a direct analog of the expression for  $c_m$  obtained by Ault *et al.* [17] in the assumption that  $\phi_s$  and  $\mathcal{Q}$  are prescribed. In our case the surface charge density is fixed, but the surface potential varies along the channel and the flow rate is established self-consistently. Once  $\mathcal{Q}$  is found,  $\mathcal{F}$  can be calculated from (50) or (54), and hence  $c_m(x)$ ,  $\psi_m(x)$ , and  $p(x)$  can be obtained.

Since  $\mathcal{Q}$  is the same at any cross-section, it may be determined by integrating Eq. (44) over  $x$

$$\mathcal{Q} = \int_0^1 \left[ u_s - \frac{\partial_x p}{3} \right] dx. \quad (58)$$

The second integral in (58) is zero since  $p(0) = p(1)$ . To calculate the first it is convenient to re-express  $u_s$  given by Eq. (48) as

$$u_s = \mathcal{F}\partial_x c_m, \quad (59)$$

where

$$\mathcal{F} = -\frac{\beta\phi_s + 4 \ln [\cosh (\phi_s/4)]}{c_m}, \quad (60)$$

is the function of  $c_m$  solely [see Eq. (22) for  $\phi_s$ ]. Equation (58) can be then transformed to

$$\mathcal{Q} = \int_0^1 \mathcal{F}\partial_x c_m dx = \int_1^{c_1} \mathcal{F} dc_m. \quad (61)$$

Thus, we have expressed the fluid flow rate in a form of the integral of  $\mathcal{F}(c_m)$  over  $c_m$ , which allows one to treat the diffusio-osmotic problems without tedious and time consuming computations. In essence, all numerical work is now reduced to the trivial calculation of this integral. In all specimen examples below to obtain  $\mathcal{Q}$  we will integrate Eq. (61) numerically (or analytically) using  $\phi_s$  calculated from Eq. (22).

From (61) it follows that  $\mathcal{Q}$  is controlled only by  $\ell_{GC}$  [that impacts  $\phi_s$ ] and  $c_1$ , but does not depend on the Péclet number or distributions of concentration (53) and pressure along the channel. In other words, to attain the high flow rate we need highly charged surfaces and a large concentration drop between reservoirs. The case of  $\mathcal{Q} = 0$  is also of much interest. It is evident that

the situation of zero  $\mathcal{Q}$  can arise from two rather different mechanisms. The first, which occurs for the uncharged surfaces ( $\phi_s = 0$ ), provides  $\mathcal{F} \equiv 0$ , so that the diffusio-osmotic flow is not induced at all. The flux of ions throughout the channel involves only their diffusion and migration. The second, which occurs for charged surfaces, involves the sign reversal of  $\mathcal{F}$ . We discuss this case further. The integral in (61) could become zero, if the function  $\mathcal{F}$  is alternating, which implies that  $\mathcal{F} = 0$  has a root in the interval of  $c_m$  from 1 to  $c_1$ . It follows from Eq. (60) that it exists only for a negative  $\beta\phi_s$ . It is possible to determine the value of  $c_1$  for a given  $\ell_{GC}$  (or vice versa) for which zero flow rate occurs by means of a construction analogous to the Maxwell one (of equal areas) employed for phase coexistence.

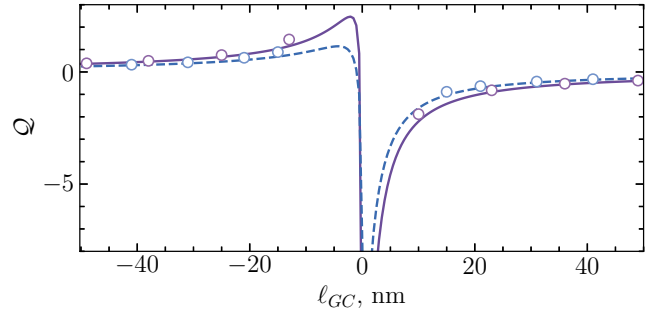


FIG. 5.  $\mathcal{Q}$  as a function of  $\ell_{GC}$  computed using  $c_1 = 10^3$  and 10 (solid and dashed curves) with fixed  $\beta = 0.5$ . Circles show calculations from Eq. (64).

By varying  $\ell_{GC}$  and calculating  $\phi_s$  it is possible to obtain the curves for  $\mathcal{Q}$  shown in Fig. 5. The calculations are made using  $c_1 = 10^3$  and 10, and for this example we fix  $\beta = 0.5$ . For positively charged surfaces the flow rate is negative [since the numerator in (60) is positive] and increases monotonically with  $\ell_{GC}$  by slowly approaching zero at large values. Since for negatively charged surfaces the numerator in (60) can take any sign depending on the value of  $\phi_s$ , the flow rate could be either positive or negative (or zero). On increasing  $\ell_{GC}$  (reducing  $|\ell_{GC}|$ )  $\mathcal{Q}$  increases nonlinearly (from zero), exhibits a maximum and then decreases sharply to a negative value becoming rather large in magnitude. It is evident that for a given  $\mathcal{Q}$  there are always two possible  $\ell_{GC}$  (and hence  $\phi_s$ ), so a great care should be taken when the measured fluid flow rate is used to infer the surface charge/potential [17, 29]. Now recall that  $\mathcal{F}$  could turn to zero, or, equivalently,  $\beta\phi_s + 4 \ln [\cosh (\phi_s/4)] = 0$ , only for negative  $\beta\phi_s$ . With  $\beta = 0.5$  the root is  $\phi_s \simeq -4.9$ . At this (sufficiently large) surface potential the electro- and chemiosmotic flow rates are significant, but they cancel out each other. Finally, we remark that the curves corresponding to different values of  $c_1$  are of the same shape, but  $\mathcal{Q}$  is slightly smaller in magnitude for smaller  $c_1$ . Thus, the data in Fig. 5 supports the above argument about an influence of  $c_1$  on  $\mathcal{Q}$ . Meantime, it can be seen that a key player in tuning

the flow rate is the surface charge density, but not the concentration drop. Finally, we note that at  $\ell_{GC} \rightarrow 0$  the surface potential diverges and this is accompanied by a divergence of  $\mathcal{Q}$ . In practice, however, it is unlikely that  $|\ell_{GC}|$  could be smaller than 1 nm [30]. Below we will use this value as a lower bound to the Gouy-Chapman length.

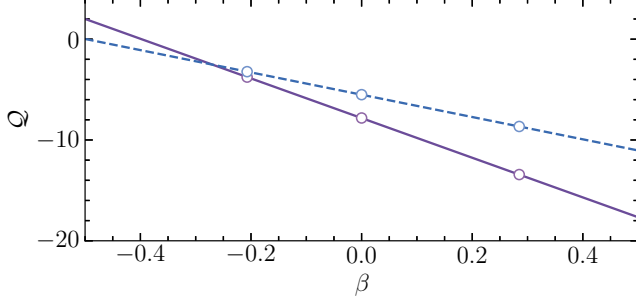


FIG. 6. The flow rate  $\mathcal{Q}$  as a function of  $\beta$  computed using  $\ell_{GC} = 1$  nm for  $c_1 = 10^3$  and 10 (solid and dashed curves). Circles from left to right mark values of  $\mathcal{Q}$  that correspond to NaCl, KCl, and  $\text{KCH}_3\text{COO}$ .

The above results for  $\mathcal{Q}$  refer to fixed (positive)  $\beta$ . If we keep  $\ell_{GC}$  fixed, but vary  $\beta$ , we move to the situation displayed in Fig. 6. The calculations are made using  $\ell_{GC} = 1$  nm and the same two values of  $c_1$  as in Fig. 5. It can be seen that the flow rate decreases linearly with  $\beta$  and the (negative) slope  $(\partial\mathcal{Q}/\partial\beta)_{\ell_{GC}}$  is larger for higher  $c_1$ . Figure 6 is also intended to illustrate that depending on  $\beta$ , the flow rate can be either positive or negative, or zero. With given parameters the zero of  $\mathcal{Q}$  that corresponds to  $c_1 = 10$  and  $10^3$  is attained when  $\beta = -0.498$  and  $-0.398$ . We have marked with symbols the flow rates that correspond to some standard salts. Recall that  $\beta$  for KCl is nearly zero, which means that electrosmosis does not emerge. However,  $\mathcal{Q}$  is large and negative, thanks to chemiosmotic flow, from “salty” towards “fresh” reservoir. For NaCl the flow rate is smaller in magnitude, but for  $\text{KCH}_3\text{COO}$  larger. The reason for this difference is clear. In the first case the emerging electrosmotic flow results in a decrement in a total  $\mathcal{Q}$  compared to the case of zero  $\beta$ , but in the second - in an increment. For these three salts the flow rate is negative, but this does not mean that a positive  $\mathcal{Q}$  cannot be attained. For example, the flow towards “salty” bath is expected for NaOH (since its  $\beta \simeq -0.596$  [26]).

Figure 7 illustrates the ion flux  $\mathcal{J}$  that corresponds to the flow rates of fluid presented in Fig. 6. The curves are calculated from Eq. (54) using  $\text{Pe} = 0.31$  obtained for  $\text{KCH}_3\text{COO}$ . However, only the rightmost circles refer to  $\text{KCH}_3\text{COO}$ ; the curves are provided simply as a guide for the eye. The left circles and the center ones refer to NaCl and KCl, and calculated using their  $\text{Pe} = 0.28$  and  $0.23$ , correspondingly. It can be seen that they are well fitted by the theoretical curves obtained at slightly higher  $\text{Pe}$ .

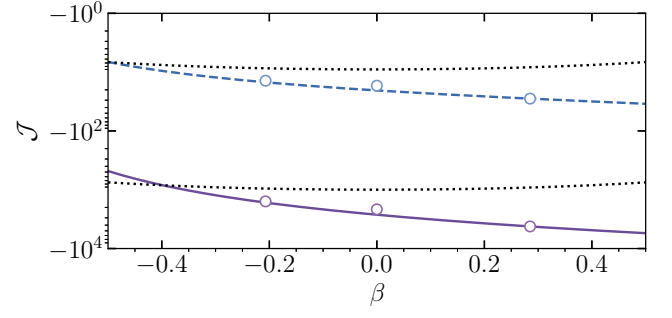


FIG. 7.  $\mathcal{J}$  vs.  $\beta$  calculated with the same parameters as in Fig. 6 using  $\text{Pe} = 0.31$  (solid and dashed curves). Circles from left to right show  $\mathcal{J}$  for NaCl, KCl, and  $\text{KCH}_3\text{COO}$ . Dotted curves are obtained using Eq. (51).

With these parameters  $\mathcal{J}$  is negative and monotonically decreases [but increases in magnitude] with  $\beta$ . It is also well seen that for a larger value of  $c_1$  the magnitude of  $\mathcal{J}$  is higher. Also included are calculations from Eq. (51), which predicts that  $\mathcal{J}$  takes its minimum value of  $1 - c_1$  at  $\beta = 0$ . It is evident that there is always an intersection of the both curves for a given  $c_1$ . In this case  $\mathcal{Q} = 0$ , so that there is no convective transfer of ions. The examples of salts in Fig. 7 correspond to a negative  $\mathcal{Q}$ , and it is well seen that in this situation the fluid flow enhances significantly the ionic flux in the direction of “fresh” bath.

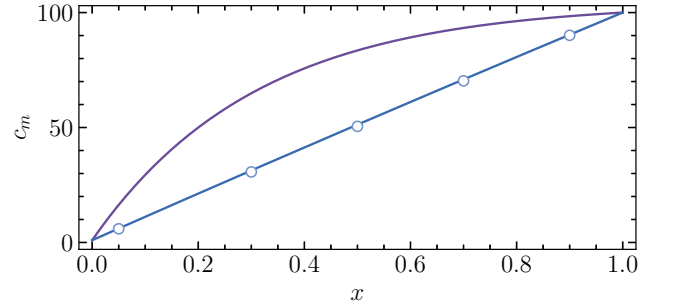


FIG. 8. Concentration  $c_m$  as a function of  $x$  for NaCl [ $\beta = -0.207$ ,  $\text{Pe} = 0.28$ ] computed using  $c_1 = 10^2$  and  $\ell_{GC} = -1$  and 5 nm (solid curves from top to bottom). Circles show calculations from Eq. (52).

The calculations of  $\mathcal{Q}$  and  $\mathcal{J}$  opened us a direct route to the determination of the concentration  $c_m$  distribution along the channel. The local  $c_m$  can be determined from Eq. (53), which reduces to Eq. (52) when  $\mathcal{Q} = 0$ . Figure 8 includes theoretical curves calculated for NaCl. The calculations are made using several  $\ell_{GC}$  from  $\pm 1$  to  $\pm 20$  nm and  $c_1 = 10^2$ , but the results are shown only for  $\ell_{GC} = -1$  and 5 nm since they constrain all other curves obtained. The concentration distributions are generally convex, that is the deviations from Eq. (52), if any, are always in the direction of larger  $c_m$ , and note that they

increase on reducing  $|\ell_{GC}|$ . For  $\ell_{GC} \geq 3$  nm the concentration curves practically merge into a straight line given by (52). An explanation can be obtained if we invoke Eq. (53). By differentiating it twice in respect to  $x$  we find that it is proportional to  $\mathcal{Q}^2[1 - \mathcal{J}/(\text{Pe}\mathcal{Q})]$ . Thus with positive  $\mathcal{J}/\mathcal{Q}$  the function  $c_m(x)$  is convex, if  $\mathcal{Q} \neq 0$ , and zero curvature is expected when the flow rate approaches to zero. The curves in Fig. 8 correspond to different values of  $\mathcal{Q}$  and  $\mathcal{J}$ . On the upper curve,  $\mathcal{Q} \simeq -11.0$  and  $\mathcal{J} \simeq -321.2$ , but for the lower one  $\mathcal{Q} \simeq 0.0$  and  $\mathcal{J} \simeq -94.5$ . So, in the former case, the flow rate is large and negative, so is  $\partial_{xx}c_m$ . In the latter case  $\partial_{xx}c_m \simeq 0$  in virtue of nearly zero  $\mathcal{Q}$ . Note that since the Gouy-Chapman length has immense variability depending on wall material and surface modification, and since  $\beta$  for some specific electrolyte can, in principle, take any value from -1 to 1, the global picture becomes rather rich. Here we make no attempt to investigate all possible scenarios for profiles of  $c_m$ , which deserves a separate publication. Instead, we simply intended to illustrate how to interpret the shape of the concentration curves using NaCl as an example.

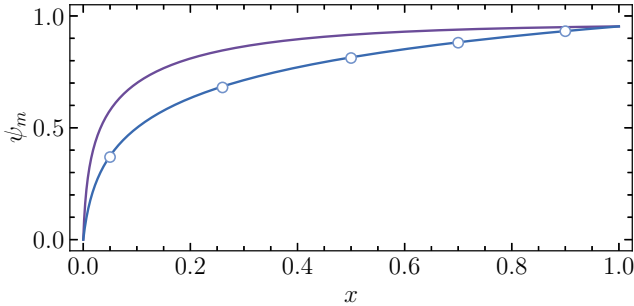


FIG. 9. Potential  $\psi_m$  as a function of  $x$  computed from Eq. (49) for the concentration profiles of NaCl displayed in Fig. 8.

The profiles of  $\psi_m$  along the channel are of interest. The calculations of local midplane potentials for the concentration distributions shown in Fig. 8 are made using Eq. (49) and included in Fig. 9. The results of calculations indicate that while convection does not affect  $\Delta\psi_m$  for NaCl, it augments the local values of  $\psi_m$  inside the channel, as well as  $\partial_x\psi_m$  at sufficiently small  $x$ . It can also be seen that the function  $\psi_m$  increases more rapidly with  $x$  close to the “fresh” end of the channel than near the “salty” reservoir. This implies that the slip velocity monotonically reduces in magnitude with  $x$  [as follows from Eqs. (47) and (48)]. Eq. (44) clarifies that in such a situation  $\partial_x p$  takes non-zero values within the channel in order to provide the same flow rate of fluid in every cross-section.

The local pressure can be obtained by integrating

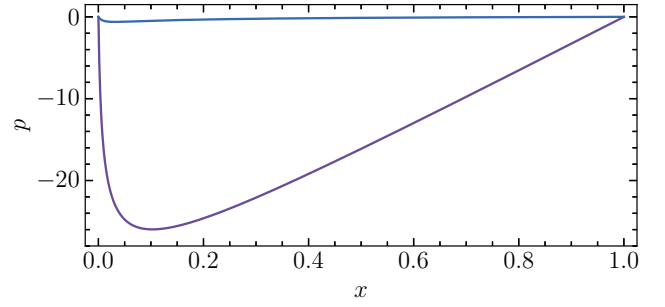


FIG. 10. The distribution of local hydrostatic pressure  $p$  along the channel computed from Eq. (62) for the concentration profiles of NaCl shown in Fig. 8. From top to bottom  $\ell_{GC} = 5$  and  $-1$  nm.

Eq. (44) from  $x = 0$  to an arbitrary  $x \leq 1$ :

$$p(x) = 3 \left( \int_1^{c_m(x)} \mathcal{F}(c_m) dc_m - \mathcal{Q}x \right). \quad (62)$$

The results of calculations are illustrated in Fig. 10. For this specimen example we again use the concentration profiles for NaCl displayed in Fig. 8. We begin with the lower curve computed using  $\ell_{GC} = -1$  nm. As  $x$  increases from 0, the pressure first decreases very rapidly and after taking its minimum value begins to augment (more slowly and linearly above  $x \simeq 0.2$ ). This implies that the pressure gradient  $\partial_x p$  is non-uniform, i.e. depends on  $x$ . Closer to the “fresh” reservoir it is large and negative, but at some  $x$  reverses its sign and finally becomes both positive and constant. There have been prior reports on such a form of the pressure curve [17, 20]. It is also seen that for a channel of  $\ell_{GC} = 5$  nm (the upper curve in Fig. 10), where  $\mathcal{Q} \simeq 0$ , the minimum of  $p$  is much less pronounced (and shifted to smaller  $x$ ). The local pressure itself is extremely small and, in essence, one can consider that it does not arise at all,  $p(x) \simeq 0$ .

### C. Velocity profiles and apparent slip

The non-uniform pressure gradient  $\partial_x p$  gives rise to a supplementary flow that has significant repercussions for the fluid velocity profile  $u_x(z)$ . The fluid velocity becomes a linear superposition of two terms: a plug diffusio-osmotic flow and the familiar parabolic profile of Poiseuille flow between parallel (no-slip) planes. Figure 11 includes theoretical curves calculated for  $x = 0.02$  and  $0.5$  with the parameters of the lower curve in Fig. 10. For these cross-sections  $c_m \simeq 6.1$  and  $77.0$ , correspondingly, but pressures are quite close ( $p \simeq -20.6$  and  $-16.1$ ). The velocity profiles are calculated from Eq. (27) with the local mobilities given by (28), (29), and (32). The local gradients are found from Eqs. (47), (53), and (62). At  $x = 0.02$  the fluid velocity plotted against  $z$

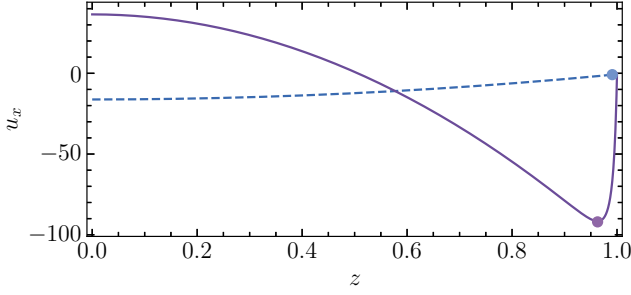


FIG. 11. Velocity profiles  $u_x(z)$  computed for the lower curve in Fig. 10 that refer to cross-sections  $x = 0.02$  and  $0.5$  (the solid and dashed curves). Circles show calculations from Eq. (59).

has a complex rippled shape with a “W-profile” (which is dubbed here the wimple by analogy to a term used to describe a rippled deformation of liquid drops [31]). This includes a large central region, where the velocity profile is convex, and an area in the neighborhood of the walls with the concave profile. Although the global flow rate  $\mathcal{Q}$  is toward the “fresh” reservoir, the very central part of fluid (near the midplane) moves away from it. The velocity reverses its sign from positive close to the midplane to negative, and after taking a minimum increases to zero at the wall. The negative area prevails since for this specific channel  $\mathcal{Q} = \int_0^1 u_x(z) dz \simeq -11$  as discussed above. At larger  $x$  this shape evolves into a conventional (concave) parabola (or “U-profile”). Our theory allows us to make contact with the simulations, which reported similar qualitative features of the evolution of velocity profile in the channel [32] and provides a direct physical explanation of this result. Since the pressure gradient reverses its sign inside the channel (see Fig. 10), the arising Poiseuille flow can be toward either “fresh” or “salty” reservoir depending on  $x$ . As  $x = 0.02$  the pressure-driven flow is directed oppositely to the diffusio-osmosis. As a result, in the vicinity of the “fresh” end we observe the wimple formation. The wimple amplitude decreases with  $x$ , and when the pressure gradient vanishes the velocity profile becomes flat. At larger  $x$  both flows are co-directed leading to the conventional parabolic profile. Its amplitude augments up to  $x \simeq 0.2$ . On increasing  $x$  further the velocity profile remains the same for every cross-section. As a side note, the analogous picture is observed if we make calculation with the parameters of the upper curve in Fig. 10, where  $\mathcal{Q} \simeq 0$ , but  $u_x(z)$  becomes much smaller in magnitude.

We now turn to the apparent diffusio-osmotic slip velocity that can be calculated from Eq. (59). In Fig. 11, we have marked with circles the quantities  $u_s$  for the corresponding curves. The locus of  $u_x(z) = u_s$  is at some distances of the order of the local Debye length [i.e.  $O(\lambda_D^* c_m^{-1/2})$ ] from the walls. Note that for the wimple profile the velocity  $u_x(z)$  takes here its minimum value.

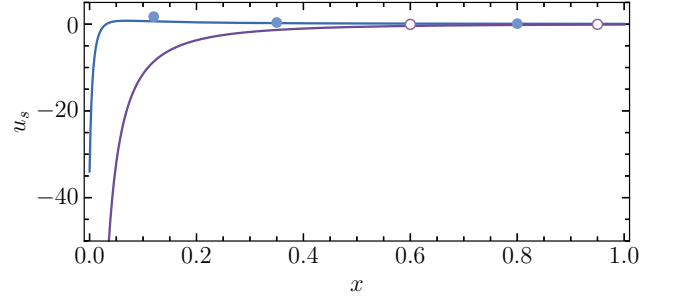


FIG. 12. Slip velocity  $u_s$  vs  $x$  computed from Eq. (59) for the concentration profiles of NaCl displayed in Fig. 8. From top to bottom  $\ell_{GC} = 5$  and  $-1$  nm. Filled circles show calculations from Eq. (65). Open circles show predictions of Eq. (63) with  $c_m$  calculated from (57) and  $\partial_x c_m$  given by (67).

By varying  $x$  and performing the same calculations we obtain the curves for  $u_s$  shown in Fig. 12. They again refer to the concentration profiles of NaCl displayed in Fig. 8. An overall conclusion from this plot is that the slip velocity  $u_s$  significantly varies along the channel. It is quite large in magnitude in the vicinity of the “fresh” reservoir, but much smaller close to the “salty” one. For the lower curve that refers to  $\mathcal{Q} \simeq -11$  the negative slip velocity monotonically reduces in magnitude with  $x$ . We emphasize that even for a channel, which is normally not regarded as highly charged and of  $\mathcal{Q} \simeq 0$ , there emerges a finite diffusio-osmotic slip that has been usually swept under the carpet. Indeed, the (upper) curve corresponds to zero  $\mathcal{Q}$ , but it can be seen that  $u_s$  is finite and alternating. The slip velocity is large and negative near the “fresh” reservoir, but small and positive in most of the channel. The nature of this is more or less apparent now. At small  $x$  the surface potential is large, so the negative chemiosmotic term in Eq. (60) dominates. On increasing  $x$  the surface potential reduces and the positive electroosmotic term becomes the leading. The integral contributions of these two terms of the opposite sign to the flow rate  $\mathcal{Q}$  given by Eq. (61) are finite, but they cancel out.

Finally, we present some analytical calculations for the case of low surface potential. From Eq. (35) it follows that when  $\phi_s \leq 1$  the electroosmotic contribution to the diffusio-osmotic velocity (the first term) is  $O(\phi_s)$ , while the chemiosmotic one (the second term) is  $O(\phi_s^2)$ . Consequently, the latter can be safely neglected. Then the slip velocity can be approximated by

$$u_s \simeq -2\beta \frac{\lambda_D^* \partial_x c_m}{c_m^{3/2} \ell_{GC}}. \quad (63)$$

By substituting the last equation into (61) we obtain the flow rate for this specific case

$$\mathcal{Q} = -4\beta \frac{\lambda_D^*}{\ell_{GC}} \left(1 - c_1^{-1/2}\right). \quad (64)$$

From Eq. (64) it follows that  $\mathcal{Q}$  is negative, if  $\beta/\ell_{GC}$  is positive, and vice versa. The calculations from (64) are included in Fig. 5. The fits are quite good for large  $|\ell_{GC}|$  (small  $|\phi_s|$ ), i.e. within the range of validity of this equation.

For  $\mathcal{Q} \leq 1$  Eqs. (53)-(55) can be expanded about  $\mathcal{Q} = 0$  and, to first order, one obtains Eq. (52) for  $c_m$ . Thus, the linear in  $x$  concentration distribution with  $\partial_x c_m \simeq c_1 - 1$  should be a sensible approximation. Substituting it to (63) we find that the slip velocity is given by

$$u_s \simeq -2\beta \frac{\lambda_D^*}{\ell_{GC}} \frac{c_1 - 1}{[1 + (c_1 - 1)x]^{3/2}}. \quad (65)$$

The calculations from Eq. (65) are compared with the results for  $\mathcal{Q} \simeq 0$  presented in Fig. 12 (the upper curve). It can be seen that (65) provides a very good fit to the numerical curve down to  $x \simeq 0.1$ . At smaller  $x$  the surface potential becomes large, so this simple analytical equation does not apply.

We remark and stress that even for small surface potentials and constant concentration gradient  $u_s$  remains a non-linear function of  $x$ . The constant slip velocity

$$u_s \simeq -2\beta \frac{\lambda_D^*}{\ell_{GC}} (c_1 - 1) \ll 1 \quad (66)$$

can be expected only if the concentration drop is extremely small,  $c_1 - 1 \ll 1$ .

For a finite  $\mathcal{Q}$  the concentration gradient is generally non-uniform, but becomes a constant when  $1 - x$  is sufficiently small. In this situation  $\phi_s$  becomes small too and  $c_m$  may be determined from Eq. (57). Differentiating this equation with respect to  $x$  we obtain

$$\partial_x c_m \simeq -\frac{(c_1 - 1)c^* \text{Pe}\mathcal{Q}}{(1 - c^*)(1 - \beta^2)} \quad (67)$$

The slip velocity  $u_s$  can then be obtained by substituting Eqs. (57) and (67) into (63). Such calculations are included in Fig. 12 and we see that they are in excellent agreement with the numerical results for a branch of the lower curve that corresponds to sufficiently small  $\phi_s$  (and a large flow rate of fluid).

## VI. CONCLUDING REMARKS

We proposed a theory of a diffusio-osmotic flow in a thick planar channel, which is valid even when the surface potential and charge density are quite large and applies at any concentration drop. The theory provides considerable insight into physics of diffusio-osmosis and has the merit of being very well suited to numerical work by dramatically simplifying it compared to prior approaches that involve a numerical solution to the system of partial differential equations. Our approach also yielded some useful analytical relations that have never been reported, and we believe we have provided satisfactory answers to

several long-standing questions formulated at the beginning of the paper.

The main results of our work can be summarized as follows. We have derived an analytical formula that relates the local “bulk” concentration  $c_m(x)$  to the flow rate of fluid  $\mathcal{Q}$  and depends on the Péclet number and diffusivities of ions. In general this varies non-linearly along the channel, that is the concentration gradient  $\partial_x c_m$  is not a constant. The slip velocity  $u_s$  is also non-uniform, so is the pressure gradient that arises naturally in our analysis providing an equal flow rate in every cross-section. We have emphasized that at a finite flow rate  $u_s$  decreases monotonically in magnitude from its largest value near the “fresh” reservoir down to the smallest in the vicinity of the “salty” one. Unexpectedly, our analysis has revealed that zero  $\mathcal{Q}$  does not necessarily imply the absence of the diffusio-osmotic flow, and can be attained when  $u_s$  becomes alternating. Finally, our exact analytical solution for the local diffusio-osmotic mobility opened a route to the determination of the local velocity profiles  $u_x(z)$ . We have clarified the evolution of their form along the channel associated with the related pressure changes.

Certain aspects of our work warrant further comments. The flow rate  $\mathcal{Q}$  is an important quantity in our theory because, in essence, it sets everything. Once  $\mathcal{Q}$  is determined, the ionic flux  $\mathcal{J}$ , local “bulk” concentrations  $c_m$  and potentials  $\psi_m$ , and hence  $u_s$  can be easily obtained by using the analytical expressions derived here. We have formulated the expression for the flow rate of fluid in the form of a simple integral that can easily be computed. It has been shown that  $\mathcal{Q}$  depends neither on the Péclet number, nor on the distribution of local concentrations along the channel being controlled only by the surface charge and (to a less extent) the concentration drop. Our identification of two separate mechanisms for vanishing of  $\mathcal{Q}$  should also be of much significance. The first, associated with zero surface potential (or charge), is, of course, well-known. The second mechanism occurs for charged surfaces and requires the alternating integrand in the equation for  $\mathcal{Q}$ . Thus, both chemi- and electroosmotic flows emerge, but their integral contributions cancel out.

One of the aims of our study was to provide fundamental theoretical understanding of some important features of diffusion-osmotic flow in a channel, which cannot be clarified from experiment, but are crucial for interpreting the data or predictive purpose. In addition to mentioned above these include such issues as the direction of the flow rate of fluid and that of the flux of ions. In particular we found that for a highly charged channel  $u_s$  is toward “fresh” reservoir, if  $\beta\ell_{GC}$  is positive. For a finite surface charge and negative  $\beta\ell_{GC}$  the slip velocity can be toward any reservoir and become even alternating. Our analysis showed that the ion flux is related to the flow rate of fluid and we clarified when and why  $\mathcal{J}$  and  $\mathcal{Q}$  become co-directed, i.e. found the conditions for the convective enhancement of  $\mathcal{J}$ . For example, the ion flux can be significantly enhanced by the fluid flow, if the latter is

toward the “fresh” reservoir and  $\beta\ell_{GC}$  is positive.

A diffusio-osmotic flow is at the origin of migration of charged particles induced by salt gradient and termed diffusiophoresis. This phenomenon represents an efficient means to efficiently manipulate the charged colloids, by inducing their spreading and focusing [33–36]. Since for particles, which radius significantly exceeds the Debye length, the same equation for  $u_s$  applies [28, 37, 38], our results may be of help at improving the description of diffusio-phoretic phenomena and devices.

The solutions derived here may also be useful for some electrochemistry areas, such as related to permeable membranes. One problem for which our work is relevant is that of the diffusion (or liquid junction) potential  $\Delta\psi_m$  associated with many practical aspects of reference electrodes, which cannot be measured directly and is difficult to interpret since the stationary state is non-equilibrium [39]. Electrochemists have long treated this potential as occurring at zero fluid flow rate. Our results show that the diffusion potential is not specific to the magnitude of  $Q$ , pointing out that the classical equation for  $\Delta\psi_m$  has validity beyond its initial assumptions. However, the real membranes are porous materials of a finite thickness and we found that the local  $\psi_m$  inside their pores is significantly affected by convection. This might have a repercussion for various applications. The same concerns the effects of a local diffusio-osmotic flow coupled with zero total flow rate that have never been considered in membrane science, but their implications could be large.

The salinity gradient has also been proposed as a source of an electric current generation [40, 41], although there are still some doubts about the efficiency

of this [42]. Our theory of diffusio-osmosis cannot be immediately applied to the description and optimisation of electric current since we have addressed the so-called an “open circuit”, where there is no electronic connection through the wires (and hence the current is zero). The approach we reported, however, could be extended for a “closed circuit” configuration. Our calculations are currently in progress for this.

As mentioned in the introduction, another avenue for driving flow on these scales is to exploit hydrodynamic slip. The later can yield considerably enhanced electro-osmotic flow in the channel (see for example [43], and references therein), as well as affects diffusio-osmosis [44]. It would be of some interest to examine the diffusio-osmotic flow between two planes by imposing the hydrodynamic slip boundary conditions. A systematic study of this kind would constitute a significant extension of our work.

## ACKNOWLEDGMENTS

This work was supported by the Ministry of Science and Higher Education of the Russian Federation.

## DATA AVAILABILITY

The data that support the findings of this study are available within the article.

## AUTHOR DECLARATIONS

The authors have no conflicts to disclose.

- 
- [1] H. A. Stone, A. D. Stroock, and A. Ajdari, Engineering flows in small devices, *Annu. Rev. Fluid Mech.* **36**, 381 (2004).
  - [2] T. M. Squires and S. R. Quake, Microfluidics: Fluid physics at the nanoliter scale, *Rev. Mod. Phys.* **77**, 977 (2005).
  - [3] R. B. Schoch, J. Han, and P. Renaud, Transport phenomena in nanofluidics, *Rev. Mod. Phys.* **80**, 839 (2008).
  - [4] L. Bocquet and E. Charlaix, Nanofluidics, from bulk to interfaces, *Chem. Soc. Rev.* **39**, 1073 (2010).
  - [5] O. I. Vinogradova, Slippage of water over hydrophobic surfaces, *Int. J. Miner. Process.* **56**, 31 (1999).
  - [6] L. Bocquet and J.-L. Barrat, Flow boundary conditions from nano-to micro-scales, *Soft Matt.* **3**, 685 (2007).
  - [7] O. I. Vinogradova and A. V. Belyaev, Wetting, roughness and flow boundary conditions, *J. Phys. Condens. Matter* **23**, 184104 (2011).
  - [8] J. L. Anderson, Colloid transport by interfacial forces, *Annu. Rev. Fluid Mech.* **21**, 61 (1989).
  - [9] S. Marbach and L. Bocquet, Osmosis, from molecular insights to large-scale applications, *Chem. Soc. Rev.* **48**, 3102 (2019).
  - [10] Z. Zhang, L. Wen, and L. Jiang, Nanofluidics for osmotic energy conversion, *Nat. Rev. Mater.* **6**, 622 (2021).
  - [11] B. Deryagin, S. Dukhin, and A. Korotkova, Diffusiophoresis in electrolyte solutions and its role in mechanism of film formation from rubber latexes by method of ionic deposition, *Kolloidn. Zh.* **23**, 53 (1961).
  - [12] D. C. Prieve, J. L. Anderson, J. P. Ebel, and M. E. Lowell, Motion of a particle generated by chemical gradients. Part 2. Electrolytes, *J. Fluid Mech.* **148**, 247 (1984).
  - [13] H. J. Keh and H. C. Ma, Diffusioosmosis of electrolyte solutions along a charged plane wall, *Langmuir* **21**, 5461 (2005).
  - [14] H. C. Ma and H. J. Keh, Diffusioosmosis of electrolyte solutions in a fine capillary slit, *J. Colloid Interface Sci.* **298**, 476 (2006).
  - [15] H. J. Keh, Diffusiophoresis of charged particles and diffusioosmosis of electrolyte solutions, *Curr. Opin. Colloid Interface Sci.* **24**, 13 (2016).
  - [16] H. Jing and S. Das, Theory of diffusioosmosis in a charged nanochannel, *PCCP* **20**, 10204 (2018).
  - [17] J. T. Ault, S. Shin, and H. A. Stone, Characterization of surface-solute interactions by diffusioosmosis, *Soft Matt.* **15**, 1582 (2019).



- [18] J. C. Fair and J. F. Osterle, Reverse electrodialysis in charged capillary membranes, *J. Chem. Phys.* **54**, 3307 (1971).
- [19] V. Sasidhar and E. Ruckenstein, Electrolyte osmosis through capillaries, *J. Colloid Interface Sci.* **82**, 439 (1981).
- [20] P. B. Peters, R. Van Roij, M. Z. Bazant, and P. M. Biesheuvel, Analysis of electrolyte transport through charged nanopores, *Phys. Rev. E* **93**, 053108 (2016).
- [21] S. Qian, B. Das, and X. Luo, Diffusioosmotic flows in slit nanochannels, *J. Colloid Interface Sci.* **315**, 721 (2007).
- [22] I. I. Ryzhkov and A. V. Minakov, Theoretical study of electrolyte transport in nanofiltration membranes with constant surface potential/charge density, *J. Membr. Sci.* **520**, 515 (2016).
- [23] S. Chanda and P. A. Tsai, Numerical investigation of diffusioosmotic flow in a tapered nanochannel, *Membranes* **12**, 481 (2022).
- [24] D. Saville, Electrokinetic effects with small particles, *Annu. Rev. Fluid Mech.* **9**, 321 (1977).
- [25] J. N. Israelachvili, *Intermolecular and Surface Forces*, 3rd ed. (Academic Press, 2011).
- [26] D. Velegol, A. Garg, R. Guha, A. Kar, and M. Kumar, Origins of concentration gradients for diffusiophoresis, *Soft Matt.* **12**, 4686 (2016).
- [27] E. S. Asmolov, T. V. Nizkaya, and O. I. Vinogradova, Self-diffusiophoresis of Janus particles that release ions, *Phys. Fluids* **34**, 032011 (2022).
- [28] T. V. Nizkaya, E. S. Asmolov, and O. I. Vinogradova, Theoretical modeling of catalytic self-propulsion, *Curr. Opin. Colloid Interface Sci.* **62**, 101637 (2022).
- [29] C. Lee, C. Cottin-Bizonne, A.-L. Biance, P. Joseph, L. Bocquet, and C. Ybert, Osmotic flow through fully permeable nanochannels, *Phys. Rev. Lett.* **112**, 244501 (2014).
- [30] O. I. Vinogradova, E. F. Silkina, and E. S. Asmolov, Surface potentials of conductors in electrolyte solutions, *J. Chem. Phys.* **161**, 204702 (2024).
- [31] L. Y. Clasohm, J. N. Connor, O. I. Vinogradova, and R. G. Horn, The “Wimple”: rippled deformation of a fluid drop caused by hydrodynamic and surface forces during thin film drainage, *Langmuir* **21**, 8243 (2005).
- [32] I. I. Ryzhkov, D. V. Lebedev, V. S. Solodovnichenko, A. V. Minakov, and M. M. Simunin, On the origin of membrane potential in membranes with polarizable nanopores, *J. Membr. Sci.* **549**, 616 (2018).
- [33] B. Abécassis, C. Cottin-Bizonne, C. Ybert, A. Ajdari, and L. Bocquet, Osmotic manipulation of particles for microfluidic applications, *New J. Physics* **11**, 075022 (2009).
- [34] P. Arya, M. Umlandt, J. Jelken, D. Feldmann, N. Lomadze, E. S. Asmolov, O. I. Vinogradova, and S. Sauter, Light-induced manipulation of passive and active microparticles, *Eur. Phys. J. E.* **44**, 50 (2021).
- [35] J. P. Ebel, J. L. Anderson, and D. C. Prieve, Diffusiophoresis of latex particles in electrolyte gradients, *Langmuir* **4**, 396 (1988).
- [36] M. Wanunu, W. Morrison, Y. Rabin, A. Y. Grosberg, and A. Meller, Electrostatic focusing of unlabelled dna into nanoscale pores using a salt gradient, *Nat. Nanotechnol.* **5**, 160 (2010).
- [37] A. Nourhani, P. E. Lammert, V. H. Crespi, and A. Borhan, A general flux-based analysis for spherical electrocatalytic nanomotors, *Phys. Fluids* **27**, 012001 (2015).
- [38] J. T. Ault and S. Shin, Physicochemical hydrodynamics of particle diffusiophoresis driven by chemical gradients, *Annu. Rev. Fluid Mech.* **57**, 227 (2024).
- [39] G. Tsirlina, Chapter 3. Liquid Junction Potentials, in *Handbook of reference electrodes*, edited by G. Inzelt, A. Lewenstam, and F. Scholz (Springer, Heidelberg, Germany, 2013).
- [40] A. Siria, P. Poncharal, A.-L. Biance, R. Fulcrand, X. Blase, S. T. Purcell, and L. Bocquet, Giant osmotic energy conversion measured in a single transmembrane boron nitride nanotube, *Nature* **494**, 455 (2013).
- [41] A. Cipollina and G. Micale, *Sustainable energy from salinity gradients* (Woodhead Publishing, 2016).
- [42] S. Lin, Z. Wang, L. Wang, and M. Elimelech, Salinity gradient energy is not a competitive source of renewable energy, *Joule* **8**, 334 (2024).
- [43] O. I. Vinogradova, E. F. Silkina, and E. S. Asmolov, Slippery and mobile hydrophobic electrokinetics: from single walls to nanochannels, *Curr. Opin. Colloid Interface Sci.* **68**, 101742 (2023).
- [44] A. Ajdari and L. Bocquet, Giant amplification of interfacially driven transport by hydrodynamic slip: diffusio-osmosis and beyond, *Phys. Rev. Lett.* **96**, 186102 (2006).